搅拌头受力模型及应用

周 利， 刘会杰， 刘 鹏
（哈尔滨工业大学 现代焊接生产技术国家重点实验室，哈尔滨 150001）

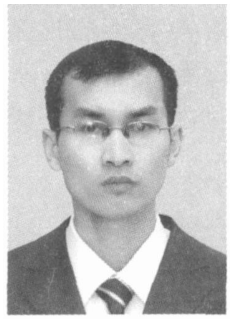

周 利

摘 要：针对搅拌摩擦焊实际过程，建立了搅拌针扎入阶段和稳定焊接阶段搅拌头的受力模型，通过与实测数据对比分析对模型进行了验证．由受力模型可知无论扎入阶段或稳定焊接阶段搅拌头的薄弱部位均为搅拌针根部，若设计不当易从搅拌针根部破坏．在此基础上，针对 Ti-6Al-4V 的搅拌摩擦焊，将模型用于指导搅拌头设计．结果表明，合理的搅拌头设计是实现钛合金搅拌摩擦焊的关键，在合适的焊接工艺参数下可以获得成形良好的焊缝．

关键词：搅拌摩擦焊； 搅拌头； 受力模型； Ti-6Al-4V
中图分类号：TG453.9 文献标识码：A 文章编号：0253－360X(2009)03－0093－04

0 序 言

搅拌摩擦焊(FSW)是近年来发展起来的一种新型固相连接技术，与传统焊接方法相比，它具有焊接质量高、生产成本低和无环境污染等优点[1－3]．鉴于其优势，该方法目前已被广泛应用于铝、镁、铜等低熔点金属及其合金的焊接．随着该技术的发展，钢、钛等高熔点材料的搅拌摩擦焊现已成为研究的热点并已取得一定进展[4－7]．

搅拌头是搅拌摩擦焊技术的核心，而其中最为关键的部分是搅拌针和轴肩，因为它们直接与被焊材料作用，搅拌头受载也来源于此．在焊接过程中，搅拌头若设计不当，在载荷作用下容易发生破坏，特别是脆性材料搅拌头更是如此．

到目前为止，关于搅拌头受力的报道很少[8,9]，而且由于搅拌头形式的多样性和焊接过程的复杂性更增加了分析的难度．文中从基本形式搅拌头入手，通过一定程度简化给出搅拌头在焊接过程中的受力模型，用于指导搅拌头设计，以防止由于设计不当而造成破坏．

1 搅拌头实体几何模型

选择图 1 所示的基本形式搅拌头作为分析对象，实际所用的搅拌针和轴肩通常开有一定形式的沟槽，以利于焊接过程产热和被焊材料流动．由于这些因素对搅拌头整体受力影响较小，在分析时将这些细节忽略．为论述的方便，将搅拌头尺寸参数用代数符号表示，具体意义将在后面给出．

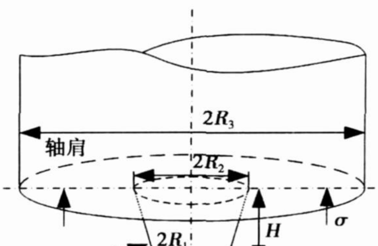

图 1 搅拌头实体模型

Fig. 1 Model of pin tool

2 搅拌头受力数学模型

2.1 焊接过程分析与简化

搅拌摩擦焊是一个非常复杂的热机作用过程，它涉及温度场、应力场和流场的交互作用．在此过程中搅拌头承受交变载荷作用，但当过程进入稳态后，搅拌头受力可以按照等效静载来分析．为简化分析，这里做如下假设：

(1) 忽略焊接过程中搅拌头 2°～5°的倾角，认为搅拌头与板面垂直．

收稿日期：2008－01－24
基金项目：大连理工大学工业装备结构分析国家重点实验室开放基金(GZ0805)；国家科技支撑计划重点基金资助项目(2006BAF04B09)；哈尔滨工业大学优秀团队支持计划资助

(2) 尽管被焊材料在焊接过程中存在流动，但是该运动相对于搅拌针的运动可以忽略不计，在分析搅拌针和轴肩与被焊材料之间的摩擦力时将其视为静止的.

整个焊接过程可分为搅拌针扎入、搅拌头前行和拔出三个阶段，由于拔出阶段搅拌头基本不受力，故只对前两个阶段进行分析，分析过程中采用移动柱坐标系.

2.2 搅拌头受力模型建立

2.2.1 扎入阶段

对于图 1 所示的搅拌头来讲，搅拌针扎入阶段假定搅拌针表面受到均布正压力作用并认为各处摩擦系数一致，则摩擦力也是均匀分布的. 搅拌针端面和侧面正压力产生平行搅拌头轴线向上的合力，摩擦力产生与搅拌头旋转方向相反的扭矩. 搅拌针端面与轴肩如图 2 所示，搅拌针侧面如图 3 所示.

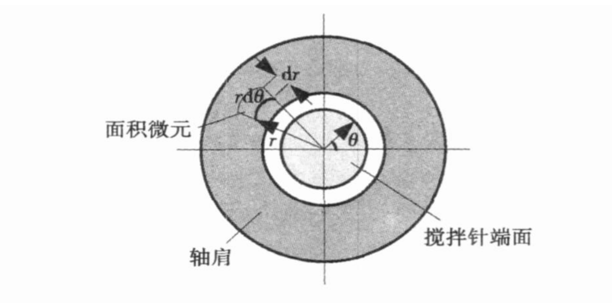

图 2 轴肩和搅拌针端面
Fig. 2 Shoulder and pin tip

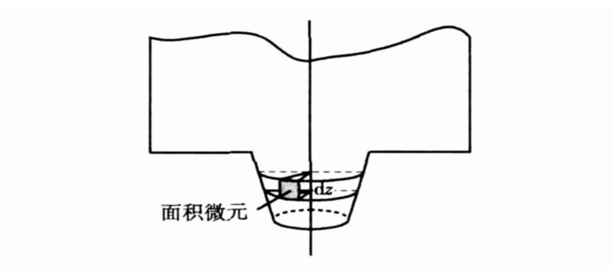

图 3 搅拌针侧面
Fig. 3 Pin side

搅拌针端面正压力产生平行搅拌头轴线向上的合力为

$$N_{pb1} = p_1 \pi R_1^2 \tag{1}$$

式中：p_1 为扎入阶段正压力；R_1 为搅拌针端面半径.

搅拌针端面摩擦力产生与搅拌头旋转方向相反的扭矩为

$$T_{pb1} = \int_0^{2\pi}\int_0^{R_1} r \times \mu_1 p_1 r \mathrm{d}r \mathrm{d}\theta = \frac{2\pi \mu_1 p_1 R_1^3}{3} \tag{2}$$

式中：μ_1 为扎入阶段摩擦系数；θ 为周向角.

搅拌针侧面正压力产生平行搅拌头轴线向上的合力为

$$N_{ps1} = \int_0^{2\pi}\int_0^{h} p_1 (R_1 + z \mathrm{tg}\,\alpha) \mathrm{tg}\,\alpha \mathrm{d}\theta \mathrm{d}z = 2\pi \sigma_1 R_1 h \mathrm{tg}\,\alpha + \pi p_1 h^2 \mathrm{tg}^2 \alpha \tag{3}$$

式中：α 为搅拌针锥度角；h 为搅拌针扎入深度.

搅拌针侧面摩擦力产生与搅拌头旋转方向相反的扭矩为

$$T_{ps1} = \int_0^{2\pi}\int_0^{h} \mu_1 p_1 \left(\frac{R_1 + z \mathrm{tg}\,\alpha}{\cos \alpha}\right)(R_1 + z \mathrm{tg}\,\alpha) \mathrm{d}\theta \mathrm{d}z = \frac{2\pi \mu_1 p_1 R h^2 \sin \alpha}{\cos^2 \alpha} \tag{4}$$

2.2.2 稳定焊接阶段

当搅拌针完全扎入并且搅拌头开始前行时，被焊材料软化并形成焊缝. 在这个过程中，搅拌针和轴肩受均布正压力作用，由于搅拌针后部与流动到其后面的高塑性软化材料接触，可以认为搅拌针侧面只有前半面上受到正压力[10]，仍假定各处摩擦系数相同. 搅拌针端面和轴肩正压力产生平行搅拌头轴线向上的合力，摩擦力产生与搅拌头旋转方向相反的扭矩. 搅拌针侧面正压力和摩擦力由于只作用在前半面上，除产生平行于搅拌头轴线向上的合力和与搅拌头旋转方向相反的扭矩外还会产生垂直于搅拌头轴线的合力. 搅拌针端面正压力产生平行搅拌头轴线向上的合力为

$$N_{pb2} = p_2 \pi R_1^2 \tag{5}$$

式中：p_2 为前行阶段正压力.

搅拌针端面摩擦力产生与搅拌头旋转方向相反的扭矩为

$$T_{pb2} = \int_0^{2\pi}\int_0^{R_1} r \times \mu_2 p_2 r \mathrm{d}r \mathrm{d}\theta = \frac{2\pi \mu_2 p_2 R_1^3}{3} \tag{6}$$

式中：μ_2 为前行阶段摩擦系数.

搅拌针侧面正压力产生平行搅拌头轴线向上的合力为

$$N_{ps2} = 2\int_{\pi}^{\frac{3\pi}{2}}\int_0^{H} p_2 (R_1 + z \mathrm{tg}\,\alpha) \mathrm{tg}\,\alpha \mathrm{d}\theta \mathrm{d}z = \pi p_2 R_1 H \mathrm{tg}\,\alpha + \frac{\pi p_2 H^2 \mathrm{tg}^2 \alpha}{2} \tag{7}$$

式中：H 为搅拌针长度.

搅拌针侧面正压力产生垂直搅拌头轴线与前行相反的合力

$$P_{ps1} = 2\left|\int_{\pi}^{\frac{3\pi}{2}}\int_0^{H} p_2 (R_1 + z \mathrm{tg}\,\alpha) \sin\theta \mathrm{d}\theta \mathrm{d}z\right| = 2 p_2 R_1 H + \sigma_2 H^2 \mathrm{tg}\,\alpha \tag{8}$$

P_{ps1} 作用在

$$h_{ps1} = \frac{-2R_1 + \sqrt{4R_1^2 + 4R_1 H \mathrm{tg}\,\alpha + 2H^2 \mathrm{tg}^2 \alpha}}{2\mathrm{tg}\,\alpha} \tag{9}$$

搅拌针侧面摩擦力产生垂直搅拌头轴线和搅拌针前行方向的合力为

$$P_{ps2}=2\left|\int_{\pi}^{\frac{3\pi}{2}}\int_{0}^{H}\mu_2 p_2\frac{(R_1+z\,\mathrm{tg}\,\alpha)}{\cos\alpha}\sin\theta\,\mathrm{d}\theta\,\mathrm{d}z\right| =\frac{2\mu_2 p_2 R_1 H}{\cos\alpha}+\frac{\mu_2 p_2 H^2\sin\alpha}{\cos^2\alpha} \quad (10)$$

P_{ps2} 作用在

$$\left.\begin{aligned} h_{ps2}&=\frac{-2R_1+\sqrt{4R_1^2+4R_1H\,\mathrm{tg}\,\alpha+2H^2\mathrm{tg}^2\alpha}}{2\mathrm{tg}\,\alpha}\\ \theta&=\frac{4\pi}{3}\end{aligned}\right\} \quad (11)$$

搅拌针侧面摩擦力产生于搅拌头旋转方向的扭矩为

$$T_{ps2}=\int_{\pi}^{2\pi}\int_{0}^{H}\mu_2 p_2\left(\frac{R_1+z\,\mathrm{tg}\,\alpha}{\cos\alpha}\right)(R_1+z\,\mathrm{tg}\,\alpha)\,\mathrm{d}\theta\,\mathrm{d}z =\pi\mu_2 p_2\left(\frac{R_1^2H}{\cos\alpha}+\frac{H^3\sin^2\alpha}{3\cos^3\alpha}+\frac{R_1H^2\sin\alpha}{\cos^2\alpha}\right) \quad (12)$$

轴肩承受的正压力合力为

$$N_{s2}=p_2\pi(R_3^2-R_2^2) \quad (13)$$

式中：R_2 为搅拌针根部直径；R_3 为轴肩直径.

轴肩摩擦力产生与搅拌头旋转方向相反的扭矩为

$$T_{s2}=\int_0^{2\pi}\int_{R_2}^{R_3}r\times\mu_2 p_2 r\,\mathrm{d}r\,\mathrm{d}\theta=\frac{2\pi\mu_2 p_2(R_3^3-R_2^3)}{3} \quad (14)$$

3　受力模型分析及验证

由受力分析可知，扎入阶段搅拌头只承受沿轴线的正压力和与旋转方向相反的摩擦扭矩，式(1)与式(3)之和、式(2)与式(4)之和分别为扎入阶段的正压力和摩擦扭矩．随扎入深度的增加两者增大，当搅拌针完全扎入时达到最大值，搅拌针根部承受最大载荷．由于实际焊接过程中搅拌针扎入速度恒定，扎入深度与扎入时间两者之间只相差扎入速度这样一个恒定的“系数”，因而正压力和摩擦扭矩随时间的变化规律与随扎入深度的变化规律一致，即两者也为扎入时间的增加而增加.

搅拌头前行过程中由于搅拌针只在前半面承受载荷，这时搅拌头除承受扭矩和正压力外，还会承受与焊接方向相反的阻力和垂直于搅拌头轴线与焊接方向的侧向力以及由它们产生的弯矩．当焊接过程进入稳态，由式(5)～式(14)可知搅拌头各部分所受载荷只与搅拌头尺寸有关，即进入稳态焊接过程这些载荷保持恒定而与时间无关.

Jackson[9] 采用传感器对基本形式搅拌头在焊接过程中的受力进行了测量(图 4)，图 4 为典型的搅拌头承载变化图，其中 F_x 为与焊接方向相反的焊接阻力，F_z 为沿搅拌头轴线的顶锻力，T 为搅拌头承受的扭矩．实测结果显示扎入阶段焊接阻力为零，顶锻力 F_z 随扎入时间(深度)的增加而增大，前述的受力分析结果与 Jackson 实测是一致的．由图 4 还可看出进入焊接阶段后，搅拌头开始承受焊接阻力．当焊接过程达到稳定后，搅拌头所受载荷基本不随时间变化而保持恒定值，采用前述受力模型所获得的结果与 Jackson 实测是一致的．与受力模型不同的是图 4 中顶锻力 F_z 在扎入停留阶段有一定程度下降随着搅拌头前行又有所回升，这是由于扎入停留时由于温度升高被焊材料软化而使顶锻力 F_z 下降，随着搅拌头前行由于前方材料尚处于“冷态”使得顶锻力上升．由于前述模型中分析的是稳态过程，所以与 Jackson 实测有出入.

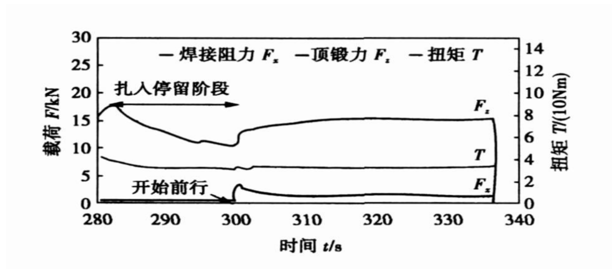

图 4　搅拌头受力变化图

Fig. 4　Load variation on pin tool

4　受力模型应用实例

根据前述的受力模型，无论搅拌针扎入过程还是搅拌头前行过程，搅拌针根部承载均比较严重，而且由于该位置为尺寸过渡处往往存在加工造成的应力集中而使其成为搅拌头的薄弱部位，特别是对于脆性材料搅拌头而言更是如此．根据前面的受力模型，主要考虑搅拌针的抗弯强度，按静载强度进行计算，并以此作为搅拌头设计的依据．针对所焊材料厚度及实际需要，可以将搅拌针长度及搅拌针锥度角先确定，但扎入阶段和稳定焊接阶段中搅拌头单位面积所受上的正压力 p_1 和 p_2 如何选取是一个关键问题，这里仍分扎入阶段和稳定焊接阶段两个阶段来考虑.

扎入过程中由于稳态温度场尚未建立，p_1 的值严格来讲是变化的，它在扎入初始阶段等于被焊材料在室温下的屈服应力．随着扎入过程的进行，由于温度的升高该值降低．由于扎入过程中产热量相对较少，在进行搅拌头尺寸设计时，p_1 应该选用被焊材料在一个较低温度下的屈服应力．这里认为此

阶段搅拌针各处温度基本相同, p_1 选用被焊材料在 0.3~0.4T_m(熔点)下的屈服强度. 搅拌摩擦焊过程进入稳态后, 若从实际过程角度考虑, 轴肩和搅拌针部分温度存在一定差异, 从应用角度出发很难建立某个很微小区域的应力分布关系而只能取一个平均应力. 稳态焊接过程中, 搅拌针和轴肩区域温度都很高, 这里将 σ_2 选为被焊材料在 0.7~0.8T_m 下的屈服应力, 因为现有报导均表明, 无论是铝、镁等低熔点材料还是钛合金等高熔点的材料搅拌摩擦焊, 稳定焊接阶段最高温度约为被焊材料熔点的 0.8 倍.

针对 2 mm 厚 Ti-6Al-4V 的搅拌摩擦焊, 根据焊接过程实际并考虑成本、加工制作等因素选择钨-铼(W-Re)合金作为搅拌头材料, 设计了图 5 所示的锥形搅拌针搅拌头. 搅拌针长度为 1.8 mm, 搅拌针根部直径为 5 mm, 在搅拌针根部设计了足够的圆滑过渡以减缓应力集中. 采用该搅拌头进行焊接试验, 焊接过程中采用氩气保护. 试验结果表明所设计的搅拌头能够顺利完成焊接过程, 在合适的焊接工艺参数下可获得良好的焊缝成形, 如图 6 所示.

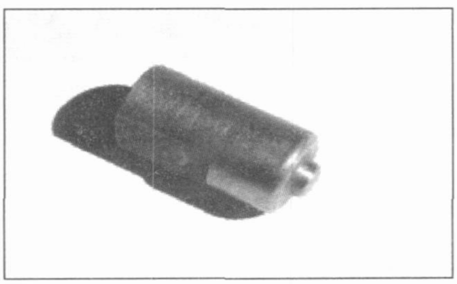

图 5 W-Re 合金搅拌头

Fig. 5 W-Re pin tool

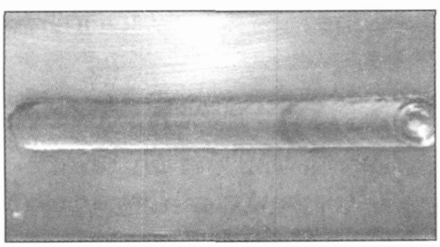

图 6 Ti-6Al-4V 搅拌摩擦焊缝

Fig. 6 Weld of Ti-6Al-4V in friction stir welding

5 结 论

(1) 针对 2 mm 厚 Ti-6Al-4V 的搅拌摩擦焊, 将模型用于指导搅拌头设计, 设计了适用于钛合金搅拌摩擦焊的搅拌头并获得了成形良好的焊缝.

(2) 简化模型的提出不仅有助于对搅拌摩擦焊过程的深入理解, 还可以为分析搅拌摩擦焊过程中的温度场、流场和应力场提供参考, 它们起相互验证的作用.

参考文献:

[1] 张 华, 林三宝, 吴 林, 等. 镁合金 AZ31 搅拌摩擦焊接头的微观组织[J]. 中国有色金属学报, 2003, 24(6): 91-96.
Zhang Hua, Lin Sanbao, Wu Lin, *et al*. Microstructure of friction stir welds in AZ31 magnesium alloy[J]. The Chinese Journal of Nonferrous Metals, 2003, 13(6): 1510-1514.

[2] 刘会杰, 陈迎春, 冯吉才. 中国搅拌摩擦焊技术的研究[J]. 焊接, 2004, (12): 5-9.
Liu Huijie, Chen Yingchun, Feng Jicai. Review of progress in friction stir welding in china[J]. Welding and Joining, 2004, (12): 5-9.

[3] Mishra R S, Ma Z Y. Friction stir welding and processing[J]. Materials Science and Engineering R, 2005, 50 (1-2): 1-78.

[4] Thomas W M, Threadgill P L, Nicholas E D. Feasibility of friction stir welding steel[J]. Science and Technology of Welding and Joining, 1999, 4 (6): 365-372.

[5] Park S H C, Sato Y S, Kokawa H K, *et al*. Rapid formation of the sigma phase in 304 stainless steel during friction stir welding[J]. Scripta Materialia, 2003, 49 (12): 1175-1180.

[6] Pilchak A L, Juhas M C, Williams J C. Microstructural changes due to friction stir processing of investment-cast Ti-6Al-4V[J]. Metallurgical and Materials Transactions A, 2007, 38A (2): 401-408.

[7] 栾国红, 柴 鹏, 孙成斌. 钛合金的搅拌摩擦焊探索[J]. 焊接学报, 2005, 26(11): 83-88.
Luan Guohong, Chai Peng, Sun Chengbin. Preliminary study on friction stir welding of titanium alloy[J]. Transactions of the China Welding Institution, 2005, 26(11): 83-88.

[8] 胡礼木, 吕晓光, 郭鹏程, 等. 搅拌摩擦焊径向阻力的动态测量与分析[J]. 机械工程学报, 2007, 43(9): 224-227.
Hu Limu, Lv Xiaoguang, Guo Pengcheng, *et al*. Dynamic measurement and analysis on radial resistant force in friction stir welding[J]. Chinese Journal of Mechanical Engineering, 2007, 43(9): 224-227.

[9] Johnson R. Forces in friction stir welding of aluminium alloys[C] // 3rd International Symposium on Friction Stir Welding, Kobe, Japan, 2001.

[10] 王大勇, 冯吉才, 王攀峰. 搅拌摩擦焊接热输入数值模型[J]. 焊接学报, 2005, 26(03): 25-28.
Wang Dayong, Feng Jicai, Wang Panfeng. Numerical model of heat input from rotational tool during friction stir welding[J]. Transactions of the China Welding Institution, 2005, 26(3): 25-28.

作者简介: 周 利, 男, 1982 年出生, 博士研究生. 主要从事搅拌摩擦焊技术研究. 发表论文 3 篇.

Email: alimse@163.com

posite bonds increases by 50% than that of the brazed bond without SiC particles. The increased strength is associated with the increase of the aluminum content and the quantity of reinforcement particles in the bond metal.

Key words: aluminum matrix composites; ultrasonically aided brazing; shear strength; microstructure; formation of composite joint

Model of forces on pin tool and its application ZHOU Li, LIU Huijie, LIU Peng (National Key Laboratory of Advanced Welding Production Technology, Harbin Institute of Technology, Harbin 150001, China). p93—96

Abstract: A model of forces on pin tool in the plunge stage and the steady welding stage during the friction stir welding (FSW) process is established and verified by comparison with experimental data. It indicates that pin root is the weakest portion of the pin tool in either the plunge stage or the steady welding stage. Pin tool can fail from the root if improper design is adopted, so the model is applied to guide design of tools for FSW of Ti-6Al-4V. The results show that proper tool design is vital to FSW for Ti-6Al-4V. Sound welds could be obtained under appropriate parameters.

Key words: friction stir welding; pin tool; model of force; Ti-6Al-4V

Characteristics of DC TIG arc with the action of a vertically incident CO_2 laser beam ZHANG Huanzhen, WU Shikai, XIAO Rongshi (Institute of Laser Engineering, Beijing University of Technology, Beijing 100022, China). p97—100

Abstract: Laser-arc hybrid welding is one of the advanced joining techniques. By using instruments such as a high-speed camera and a laser power meter, the effects of a vertically incident CO_2 laser beam on characteristics of a DC tungsten inter-gas arc are investigated. Results demonstrate that the laser-arc interaction causes the curve of arc static characteristic to shift downwards, the arc column to expand, the electric power to decease and the total arc power increase. With the increase of the laser power, the downward shift of the static characteristic curve increases, but the total arc power increases. The lower the arc current is and the nearer the laser beam locates to the cathode, the more the arc voltage decreases, which the expansion of the arc column mainly occurs in the range between the laser beam location and the anode.

Key words: tungsten inter-gas; CO_2 laser; static characteristic of arc; arc configuration; arc power

Fatigue analysis of welded joints by method of structural stress WU Qi, QIU Huiqing, WANG Weisheng (Department of Mechanical Engineering, Tongji University, Shanghai 201804, China). p101—105

Abstract: Based on the structural stress method, some data of the fatigue strength of 16Mn, which include non-carrying-load fillet cruciform joints, carrying-load fillet cruciform joints and welded joints with longitudinal fillet welded gusset, are analyzed. The discrete structural stress formula which suits for finite element method are deduced, structural stress concentration factors for joints are obtained, and structural S-N curves for these joints are provided. The approach shows the good mesh-size insensitive characteristics. Compared with the nominal stress method, the dispersity of experimental data evaluated by structural stress method is reduced.

Key words: welded joints; fatigue assessment; structural stress

Spectra analysis and temperature measure of plasmas in YAG-MIG hybrid welding of 5A90 GUO Li[1], DUAN Aiqin[2], YU Yousheng[1] (1. School of Material Science and Engineering, Wuhan University of Technology, Wuhan 430023, China; 2. National Key Laboratory of High Energy Density Beam Processing Technology, Beijing Aeronautic Manufacturing Technology Research Institute, Beijing 100024, China). p106—108

Abstract: The spectra of vapor/plasmas were acquired by spectrometer during YAG-MIG hybrid welding of 5A90 Al-Li alloys in our research. The temperature values of the vapor/plasmas were calculated by the methods of relative intensity. The effects of arc current and heat input on the temperature of the vapor/plasmas were discussed. The results show that the spectra of hybrid welding in the range of 350—850 nm is mainly argon ion spectra line accompanied with a few Mg and Li ion. An average temperature under a set of processing parameters is 6554 K; compared to YAG welding, the value has an increase of 1200 K; however, it is near to the average temperature of MIG welding.

Key words: YAG-MIG hybrid welding; metal vapor/plasmas; spectrum

3-D numerical simulation of welding spherical valve core DING Hui, LEI Junxiang, ZHU Hanhua, LI Xinran (University of Shanghai for Science and Technology, Shanghai 200093, China). p109—112

Abstract: Welding is the key course in manufacturing the spherical valve core through steel tube's necking, assembling, welding and grinding. Because the necked workpiece is under stress before welding and is to be prepared for grinding after welding, how to choose sound welding parameters so as to control residual stress with the precondition of excellent weld quality becomes the focus of this paper. A series of numerical simulations which show the real-time dynamic changes under different welding parameters for necked workpiece are demonstrated, and the optimization parameters are obtained through comparing the welding size and residual stress after welding. Analysis and illustrations on the accumulated results show that the residual stress after welding is overlapped in the former procedures.

Key words: spherical valve core; necking; numerical simulation; parameter optimization